Status of a Silicon Lattice Measurement and Dissemination Exercise

Richard D. Deslattes and Ernest G. Kessler, Jr.

Abstract—**Although no longer explicitly directed toward measurement of the Avogadro constant, we continue significant effort on lattice period measurement in monocrystalline silicon. There are currently operating an upgraded x-ray/optical interferometer and a recently established lattice comparator. We report the status of measurements with these two instruments.**

Background

NEARLY twenty years ago three groups at NBS (now NIST) participated in a re-determination of the Avogadro constant [1], [2]. Our efforts, in common with those which continue elsewhere, including those reported at this Conference [3]–[5], entailed: optical interferometry of the spatial period of a Si monocrystal, density determination using dimensionally standardized artifacts, and determination of the mean molar mass of the specimens from absolute isotopic abundance measurements. As understood at the time [1], the error budget was dominated by imprecision and inaccuracy in density and mean molar mass. Later the lattice spacing measurement was called into question by subsequent work at PTB which showed a 1.8 ppm difference from the NBS result [6], [7].

In order to investigate possible origins of this discrepancy, the NBS x-ray/optical interferometry experiment, XROI, was re-established in 1984 with several technical improvements, including frequency controlled scanning of x-ray fringe profiles and on-line, interferometric trajectory measurement. (In the earlier measurements, trajectory data were inferred in two stages: pitch errors were estimated on-line from fringe contrast while yaw motion was evaluated subsequently by use of a narrow diffraction feature.) In early 1986, the new trajectory measurement capability pointed to the fact that previously observed fringe contrast constancy did not adequately assure absence of pitch motion during the measurement [8]. It also became clear that the geometrical alignment techniques used in the past, though sufficient in the absence of pitch error were not so for the values found. Subsequent study provided a semi-quantitative accounting for the 1.8-ppm discrepancy and led to a situation of general concordance between the NBS and PTB results [9].

Data emerging during this investigative phase suggested that accuracies better than 0.1 ppm were possible in principle. With further progress in the other aspects of the Avogadro constant work, such improvements will become relevant, while even today such accuracy levels could make meaningful contributions to determination of $N_A h/c$ by diffraction spectroscopy and mass spectroscopy [10]. Also, as it becomes possible to obtain x-ray spectra from cooled samples of one- and two-electron heavy ions, their narrow natural linewidths and potential for high precision tests of basic physical theory make these attractive objects for precision spectroscopy based on a measurement chain connected to the Rydberg constant. In each of these cases, it is desirable to provide a convenient means for dissemination of XROI results to other specimens whose sizes and shapes are optimized for the respective applications.

To address this requirement, we have established a differential measuring engine, the DELTA-d machine, which has been optimized for the intercomparison of crystal specimens having nearly equal lattice periods at a level of imprecision smaller than the target accuracy of the absolute spacing measurements. The general approach to avoiding apparent limitations due to x-ray linewidths was already suggested by Hart [11] although he did not initially exploit the diffraction fine-structure which gives this method its greatest promise. Our efforts in this area have led to a comparator equipped with high performance interferometric angle measurement facilities and have required development of sample preparation, characterization, and support procedures that are more refined than one might have initially thought necessary. Similar methodology but with autocollimator angle measurement has been used at the PTB [7], [12].

Present Status of the XROI Experiment

This section addresses certain features of the "new" XROI experiment and data which have thus far emerged. Like its predecessor, the current experiment is contained in a heavy-walled aluminum vacuum box which is now held at low pressure by a large ion pump. The vacuum box is surrounded by a thermal enclosure, the whole being atop an air-spring supported granite table which, in turn, is contained in an acoustically damped compliant enclosure. Within the latter enclosure but external to the first thermal shield are the three laser systems used for optical measurements of displacement and trajectory curvature along with x-ray detectors. The x-ray source(s) are external to the isolated regions and mounted on the room wall independently of the vibration isolated platform. This arrangement, though obviously advantageous from the viewpoint of noise and vibration, places severe requirements on the positional stability of the granite table; these requirements are adequately met by a system of proximity detectors and electronic servos controlling gas supplied to the supporting air-springs [13]. The granite table and its supports stand atop an isolated pier in an underground room closed by double doors; all controls and personnel are restricted to an adjoining room. Even with these precautions, cultural noise from the control room is evident in easily monitored signals as are contributions from nearby traffic and wind-driven motion of an adjoining building.

Manuscript received June 13, 1990; revised September 21, 1990.

The authors are with the National Institute of Standards and Technology (NIST), Physics, A141, Gaithersburg, MD 20899.

IEEE Log Number 9041847.

U.S. Government work not protected by U.S. copyright

Principal Features of New XROI

The current experiment differs from its predecessor mainly by the addition of two new laser systems and extensive computer automation. One of the laser systems is a broadly tuneable local oscillator that is frequency-offset-locked to the iodine stabilized HeNe laser which remains as the system standard, see Fig. 1(a). In operation, the optical Fabry–Perot component of XROI is servo-locked to the local oscillator laser while the latter steps through a frequency excursion large enough to cover more than a complete x-ray period. The second laser system is a single frequency device whose output is divided into four beams that proceed through a polarizing beam splitter to two auxiliary mirrors on the mechanical scanning device as indicated in Fig. 1(b). The two-beam interference signals, after polarization encoding and decoding optics are pair-wise subtracted to obtain electrical measures of pitch and yaw motion (the difference signals are zero for rectilinear translation, nonzero values indicating pitch and yaw error in that motion). Both the local oscillator laser and the trajectory measuring laser are isolated from optical feedback by acoustooptic modulators operating near 70 MHz. In the case of the frequency agile local oscillator laser, RF power to the AO modulator is controlled to yield a ''leveled'' optical output. The local oscillator laser is also frequency modulated (at 7 kHz) to obtain the discriminant signal needed to lock the FP cavity to its mean frequency.

Although this report is of a skeletal character, it seems appropriate to mention the procedures used for temperature measurement and control. Room air enters through small holes in the ceiling and exhausts at floor level; a wall-mounted thermoregulator is well tuned and subject to driven air flow. Overall this ambient control seems to perform at the level of 0.1 °C over a 24 h period although larger changes occur in response to weather conditions. The next level of control comes from a thermistor sensor on the granite and a small distributed heater under this slab. The final level of measurement is from a group of four thermistors in contact with various parts of the scanning mechanism; two, which are close to the silicon crystal's two components, are seen to drift by millidegrees in 24 h after equilibration which takes about 3 days. The thermistors were independently calibrated to near the millidegree level and are periodically checked against one another by inserting them into a hole in a copper block.

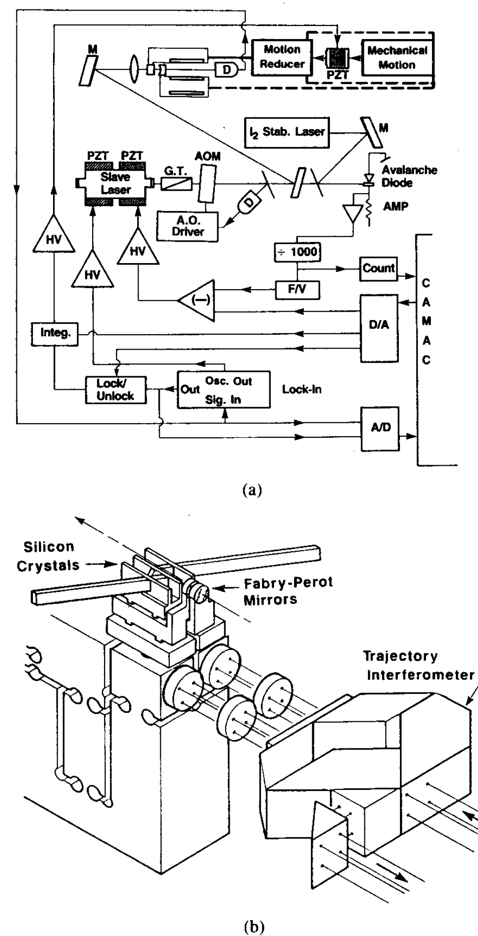

Fig. 1. Features of the new XROI experiment: (a) Local oscillator control and cavity-locking scheme. (b) Trajectory interferometer optics shown in relation to x-ray and optical measurement systems.

Outline of Data Acquisition Procedures

Measurements with XROI entail excursions of up to about 280 optical orders which are traversed in successively opposite directions over a period of 10 to 20 h. The usual number of round-trips has been five, while optical fringe steps have ranged from 3 to 36. Typically, we have made use of 2 to 18 optical order intervals with 24 to 12 measurement points in each one-way trip. At each measurement point, x-ray phase (at a nominal offset frequency of 425 MHz) is determined by x-ray intensity measurements (typical counting time is 4 s) at a set of offset frequencies beginning at 425 MHz, increasing to 650 MHz, decreasing to 200 MHz, and finally returning to 425 MHz, with a total of 25 observations; signals associated with pitch and yaw as well as temperature are acquired at the same time. The mean x-ray counting rate of 2000 Hz gives near 1–2% statistics at each point (actually the x-ray intensity varies from below 1000 cps to above 3000 Hz, i.e., fringe contrast in excess of 50%). The primary observable is the phase of the x-ray interference signal at 425 MHz which comes from fitting the x-ray intensity versus offset frequency.

Electrical values of pitch and yaw error require conversion factors before their effect on the x-ray phase can be estimated. These calibration coefficients are determined in separate experiments where the pitch or yaw angle is systematically varied. From fitting the x-ray phase as function of the pitch (yaw) electrical signal, one extracts coefficient RFAC (DFAC) which, combined with electrical pitch (yaw) signals, correct the observed x-ray phases for trajectory curvature. A further correction to observed phase data are required to account for the nonuniform spacing of adjacent modes in the (hemispherical) F-P cavity. This correction amounts to: $[\arcsin(L/R)]/\pi$ and requires separate evaluation of the absolute cavity length, L, and the radius, R, of the spherical mirror. Evaluation of R proceeds from determination of the intermode spacing of off-axis modes under deliberately mismatched conditions. L emerges from the laser frequency change needed to scan an x-ray period. One easily sees that this is equivalent to determination of the cavity's free spectral range, $c/2L$, since to the needed approximation, the spatial ratio of the optical interval, $\lambda/2$, to the lattice period, d, is already well known.

Trajectory Characterization and Control

As noted above, electrical data representing pitch and yaw error are recorded along with the x-ray intensity and offset frequency measurements in the normal course of a measurement cycle. These data, when combined with the separately determined coefficients relating x-ray phase to these electrical signals suffice, in principle, to determine the trajectory of motion. The refinement needed is of the order of 0.2 nanoradian, which corresponds to optical fringe interpolation to the 0.01 millifringe level. To reach this domain, we use an analysis procedure which is able to penetrate the apparent noise floor in a fashion analogous to the operation of a lock-in amplifier [14]. Specifically, after averaging the tilt signals at each of the optical orders used, the ensemble of trajectory data is resolved into position-dependent and time-dependent components. The latter component is taken to be smooth and fitted to a polynomial, while the former is assumed constant over a day's data run. These smoothed components are then combined to obtain a noise-filtered representation of the effective trajectory plus temporal drift. An ambiguity remains as to whether the drift term is real or associated with the path-measuring interferometer; indirect evidence suggests that, under well-equilibrated conditions, the indicated drifts are mostly real. To address this point, the experiment has been fitted with piezoelectric correctors which can be programmed to remove most of the trajectory errors or to exaggerate them. Our initial studies of data taken in adjacent time frames with and without operation of the correctors suggest that these procedures appear reliable but further systematic study is needed. Although trajectory corrections are quite serious, it should be noted that their sizes are typically below the 1-ppm level.

Characteristics of Currently Available Data

When corrections for trajectory error and diffraction phase shift have been taken into account, one expects that x-ray phase data should progress uniformly with the distance moved. The slope of such a presumably straight line is, in fact, the primary output datum since it is a measure of the ratio of the optical half-wavelength to the x-ray period modulo of its greatest integer part. Over the past year, our interest has focused on the residues from this linear model. As shown in Fig. 2(a) for a typical run, these residues exhibit surprising regularity. Such regularity is seen in all data obtained thus far and invites a statistical analysis based on asking what part of the observed residue pattern is reproducible over the round-trip excursion and what part is random or at least irreproducible. The result of such an analysis is shown in Fig. 2(b) which might be taken as representing the intrinsic limiting quality of the measurement procedure. The approximately 0.01 radian (of x-ray phase) should be considered in relation to the total excursion of 2 000 000 x-ray radians as indicating a limiting precision of the order of 0.01 ppm or better. Such a result can in no way be claimed in view of the much larger systematic residue pattern, which remains completely unexplained at the present time.

In addition to the unexplained and prominent residue pattern, data to date have other problems as well. Chief among these is that, when finally reduced to obtain crystal spacing values, the results wander about over a range of almost 0.3 ppm even though individual error estimators are much smaller than this, typically nearly tenfold. Of course, in the presence of the above-noted systematic residue patterns, the significance of statistical measures of error cannot be asserted. In fact, one is tempted to associate these two problems with one another, although this need not be the case at all. It should be noted, however, that even with the full range of variability indicated, lattice parameter values emerging from current work in this laboratory remain generally consistent with the earlier results from the PTB and the exchanged sample intercomparisons described below.

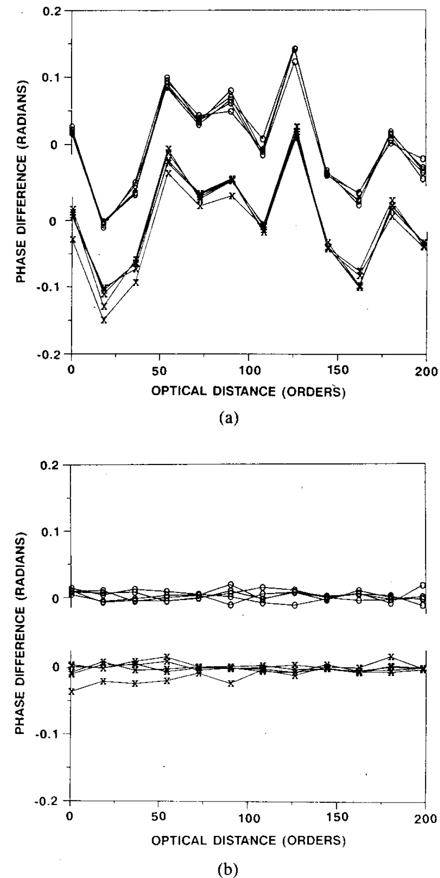

Fig. 2. Sample of data from XROI shown as residues from predicted x-ray phase advance versus optical order: (a) Total residues for five round trips, northbound leg "o", southbound "x". (b) Residues from reproducible component of (a), an indication of random error level.

General Features of the DELTA-d Spectrometer

The principle of the NIST lattice comparison measurement is illustrated by the geometrical layout of the DELTA-d spectrometer shown in Fig. 3(a). This spectrometer is a conventional double crystal Laue-case geometry used only in the nondispersive mode. Lattice spacing comparisons using similar geometries are discussed in [7], [15]–[17]. The unique features of this spectrometer are a precision angle measuring interferometer, rapid interchange of crystal samples, and crystals whose thicknesses have been chosen so that the x-ray profiles have fine structure oscillations.

X-rays from the two sources alternately proceed along paths 1 (dot) and 2 (dot, dash) to the detectors. Profiles are recorded by rotating the long first crystal. If the crystal planes at the two

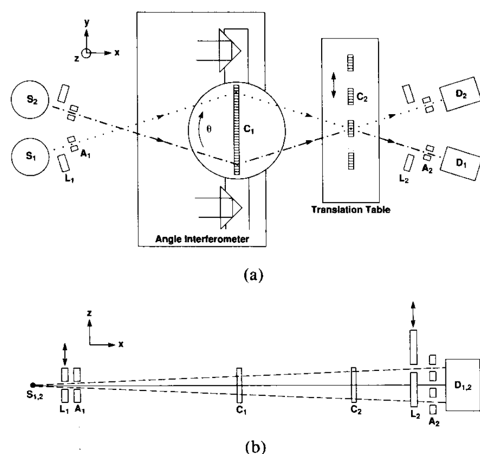

Fig. 3. Top view (a) and side view (b) of DELTA-d spectrometer: $S_{1,2}$—x-ray sources: $L_{1,2}$—shutters; $A_{1,2}$—apertures; $C_{1,2}$—crystals; $D_{1,2}$—detectors.

ends of the first crystal are parallel and the lattice spacing of the first crystal equals that of the second crystal (also called the standard crystal because its lattice spacing is known), then the profiles recorded by the two detectors will peak at the same angular setting of the first crystal. In general, the first crystal does not satisfy the above conditions and the two profiles are separated by a small angular offset, β_s (typically < 0.05 arcsec). Next, a second small crystal, whose lattice spacing is unknown, is brought into the position where the x-ray beams diffracted by the first crystal intersect. Another set of profiles is recorded by rotating the first crystal and an angular offset, β_u, is determined. By subtracting the angular offsets measured with the different second crystal samples, the properties of the first crystal are eliminated. The first crystal thus serves only as a temporary reference and its properties need be constant only for the time required to measure two different second crystal samples (a few hours).

The difference in lattice spacing $\Delta d = d_s - d_u$ is given by

$$\Delta d/d = -\tan\theta(\beta/2) \qquad \text{where } \beta = \beta_s - \beta_u$$

For $\Delta d/d = 1 \times 10^{-8}$ and $\theta = 16°$ (Ag Kα and Si 440), $\beta =$ 0.001 arcsec. A typical data sequence involves many changes of crystal samples and permits compensation of drifts of the crystals relative to the angle measuring interferometer.

Some Details of the DELTA-d Spectrometer

The radiation sources are identical silver or molybdenum x-ray tubes. They and the detectors can be positioned for Bragg angles of 10 to 22°. Lead shutters, L_1, near the source slits are computer controlled to block and pass the x-ray beams so that the two profiles can be recorded almost simultaneously. The slits are centered on the plane of dispersion using well-established mechanical and optical tooling procedures. X-ray diffraction through slits, A_2, near the detectors which are above and below the plane of dispersion provide a diagnostic for adjusting the tilts of the second crystals so that their planes are parallel to those of the first crystal (see Fig. 3(b)).

Angles are measured by a heterodyne laser Michelson interferometer having a sensitivity of a few of 10^{-4} arcsec. The interferometer is illuminated by a commercial 2-frequency HeNe laser which emits two orthogonal linearly polarized frequencies separated by 1.8 MHz. A polarization sensitive beam splitter isolates a single frequency and polarization in each arm of the interferometer. Two corner cubes, mounted on an arm which is rigidly attached to the rotating table and crystal, retro-reflect the light. A frequency difference signal from the interferometer output beam is compared to the frequency difference signal for the light emitted by the laser. For a stationary interferometer the two difference frequency signals are identical except for phase. Rotation of the interferometer arm changes the phase between the two difference frequencies, and rotation angles are determined by measuring phase change.

Heterodyne Michelson interferometers have been shown to be nonlinear due to imperfect separation of the two frequencies [18], [19]. Recently, we have measured the nonlinearity of a heterodyne interferometer similar to the one used on the DELTA-d machine. By tipping the polarizing beam splitter, the amount of mixing of the two frequencies in the interferometer arms can be varied. For large misalignments (1–2°) between the beam splitter axes and the laser beam polarization directions, nonlinearity as large as 0.015 optical fringes has been measured. However, for good alignments, the nonlinearity is reduced to 0.0025 optical fringes, which corresponds to an error of 0.003 ppm in $\Delta d/d$.

Crystal Preparation

As mentioned above, an angular offset of $\beta = 0.001$ arcsec translates into $\Delta d/d = 1 \times 10^{-8}$. Since the full width at half maximum (FWHM) of a nondispersive x-ray profile obtained with Ag Kα and Si 440 is ~ 0.6 arcsec, the profile peak positions need to be determined to 1/500 of the FWHM in order to approach 0.01 ppm. By carefully matching the thicknesses of the first and second crystals to within a few microns, nondispersive Laue-case rocking curves exhibit oscillatory fine structure which is less than 1/10 as wide as the FWHM of the profile [20]. This fine structure serves as a series of sharp convenient references to measure the angular separation of the x-ray profiles recorded in the two paths. The crystals are cut with a diamond saw and then polished to the desired thickness using a combination chemical etch, optical grinding solution. Crystal thicknesses are measured with a three coordinate measuring machine with an uncertainty of 1–2 microns and the crystal thicknesses are matched to within 2–4 microns. We have used a crystal thickness of 0.455 mm for most of our measurements as a compromise between x-ray intensity and practical problems encountered in the preparation of thin crystals. Theoretical and experimental profiles for this thickness are shown in Fig. 4.

In order to reduce strains, the crystals are made with a thick base (1.5 cm wide × 1.5 cm high) on top of which is a thin wafer that is used for diffraction. Typical lengths of the long and short crystals are 6.3 cm and 1.5 cm, respectively. Mounting is by means of a low temperature optician's wax at the central balance point.

Preliminary Comparison of PTB and NIST Samples

Two sample crystals were prepared with thicknesses near 0.455 mm from Si material supplied by PTB and NIST. The PTB material was labeled WASO 17 while the NIST sample was material adjacent to the NIST XROI crystal. An individual lattice comparison of these two crystal samples typically con-

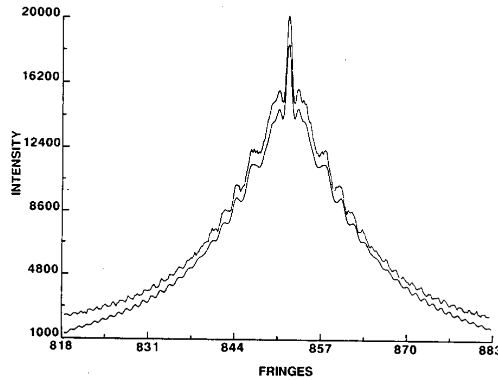

Fig. 4. Experimental (upper) and theoretical (lower) profiles for Si 440 reflection of Ag Kα radiation and crystal thickness = 0.455 mm.

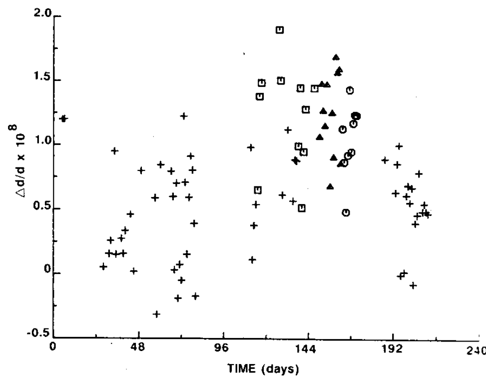

Fig. 5. Comparison of NIST and PTB crystals: + Ag Kα, first crystal 0°; □ Ag Kα, first crystal 180°; ⊙ Mo Kα, first crystal 0°; Δ Mo Kα, first crystal 180°.

sisted of 16 to 20 data scans preceded and followed by alignment scans. The alignment scans check the parallelism of the planes of the first and second crystals. The profiles were scanned by repeating the following sequence: unknown crystal—cw rotation, unknown crystal—ccw rotation, standard crystal—cw rotation, and standard crystal—ccw rotation. After determining the angular separation for each scan, the angular separations versus time for each crystal are fit with a polynomial and the angular offset between these two curves is the angular offset between the unknown and standard crystals for one data set. The scatter in the angular offsets was typically $< 6 \times 10^{-9}$ radians, provided the crystals were well aligned and the same areas of the crystals were used.

In order to test the reproducibility of the Δd measurements and to identify systematic error components, these same two crystals were compared using Ag Kα and Mo Kα x-ray radiation and with the long crystal in the two possible orientations (the 0° and the 180° orientation). In Fig. 5 the measured values of $\Delta d/d$ versus time are plotted using different symbols for the different sources and the different first crystal orientations. The average numerical values for the different sources and first crystal orientations are presented in Table I. The scatter in the data as seen in both the table and the figure suggests that the $\Delta d/d$ measurements are troubled by systematic effects related to the source and the first crystal orientation which have a magnitude <0.01 ppm. If each of the entries in the table is considered as an independent measurement, then an average difference of $\Delta d/d$ ((NIST–WASO 17)/NIST) = $1.037 \pm 0.341 \times 10^{-8}$ is obtained.

TABLE I
COMPARISON OF PTB AND NIST SAMPLES

Source	First crystal Orientation	$\Delta d/d \times 10^8$*
Ag Kα	0	0.508 ± 0.379
Ag Kα	180°	1.236 ± 0.393
Mo Kα	0	1.050 ± 0.262
Mo Kα	180°	1.251 ± 0.310

*$\Delta d/d$ = (NIST-PTB)/NIST

In a measurement done at PTB, $\Delta d/d$ for WASO 17 versus WASO 4.2A (the PTB x-ray interferometer sample) was measured to be $2.5 \pm 1 \times 10^{-8}$ (WASO 17 > WASO 4.2A) [21]. A value of $\Delta d/d$ ((NIST–WASO 4.2A)/NIST) $\sim 3.5 \times 10^{-8}$ is obtained by combining these two results. This value needs to be regarded as preliminary until additional systematic errors are evaluated. However, a final uncertainty near 1×10^{-8} appears to be possible from our lattice comparison technique.

ACKNOWLEDGMENT

The work reported has benefitted from the helpful collaboration of Muhammad Arif in the XROI experiment and M. Scott Dewey in DELTA-d, while Albert Henins made valued contributions to both effects. At earlier times, the authors enjoyed the participation of Mitsuru Tanaka, Lars Nielsen, and Gao Weibin.

Note Added in Proof: Subsequent replacement of the Fabry–Perot mirrors (one of which showed coating separation from its substrate) yielded residues free of the patterns described in this report. On the basis of a very few initial data runs it appears that the structured residue problem is no longer a limiting factor in these measurements.

REFERENCES

[1] R. D. Deslattes *et al.*, "Determination of the Avogadro constant," *Phys. Rev. Lett.*, vol. 33, pp. 463–466, Aug. 1974.

[2] ——, "Avogadro constant—corrections to an earlier report," *Phys. Rev. Lett.*, vol. 36, pp. 898–900, Apr. 1976.

[3] P. Seyfried, "Molar volume of silicon, avogadro constant-atomic mass standard, recent results-perspectives," presented at CPEM '90, Ottawa, Canada, June 11–14, 1990.

[4] G. Basile, *et al.*, "An experiment in x-ray interferometry: accuracy and resolution in Si d[220] determination," *IEEE Trans. Instrum. Meas.*, vol. 40, pp. 98–102, Apr. 1991; A. Peuto and A. Sacconi, "Volume and density measurements for the IMGC Avogadro experiment," *IEEE Trans. Instrum. Meas.*, vol. 40, pp. 103–107, Apr. 1991.

[5] K. Nakayama *et al.*, "A combined x-ray and optical interferometer with a new translation stage," *IEEE Trans. Instrum. Meas.*, vol. 40, pp. 108–109, Apr. 1991.

[6] P. Becker *et al.*, "Absolute measurement of the (220) lattice plane spacing in a silicon crystal," *Phys. Rev. Lett.*, vol. 46, pp. 1540–1543, June 1981.

[7] ——, "The lattice parameter of highly pure silicon single crystals," *Z. Phys. B*, vol. 48, pp. 17–21, 1982.
[8] R. D. Deslattes *et al.*, "Remeasurement of a silicon lattice period," *IEEE Trans. Instrum. Meas.*, vol. 36, pp. 166–169, June, 1987.
[9] R. D. Deslattes, "X-ray interferometry and gamma-ray wavelengths," in *The Art of Measurement*, B. Kramer, Ed. Weinheim, Germany: VCH Verlagsgesellschaft, 1988, pp. 193–208.
[10] R. D. Deslattes and E. G. Kessler, Jr., "Precision gamma- and x-ray energies," in *Atomic Masses and Fundamental Constants*, vol. 6, J. A. Nolan, Jr. and W. Benenson, Eds. New York, NY: Plenum Press, 1979, pp. 203–218.
[11] M. Hart, "High precision lattice parameter measurements by multiple Bragg reflection diffractometry," in *Proc. Roy. Soc. Lond. A*, vol. 309, pp. 281–296, 1969.
[12] H. Siegert *et al.*, "Determination of silicon unit cell parameters by precision measurements of Bragg plane spacings," *Zeits. f Phys. B*, vol. 56, pp. 273–278, 1984.
[13] G. L. Greene, "Accurate positional servo for use with pnuematically supported masses and vibrationally isolated tables," *Rev. Sci. Inst.*, vol. 58, no. 7, pp. 1303–1305, 1987.
[14] The basic algorithm was developed in collaboration with James Filliben of the Center for Applied Mathematics at NIST.
[15] M. Ando *et al.*, "A simple Bragg-spacing comparator," *Acta Cryst. A*, vol. 34, pp. 484–489, 1978.
[16] D. Windisch and P. Becker, "Lattice distortions induced by carbon in silicon," *Phil. Mag. A*, vol. 58, no. 2, pp. 435–443, Aug. 1988.
[17] D. Hauserman and M. Hart, "A fast high-accuracy lattice parameter comparator," *J. Appl. Cryst.*, vol. 23, pp. 63–69, 1990.
[18] C. M. Sutton, "Non-linearity in length measurement using heterodyne laser Michelson interferometry," *J. Phys. E: Sci. Instrum.*, vol. 20, pp. 1290–1292, 1987.
[19] N. Bobroff, "Residual errors in laser interferometry from air turbulence and nonlinearity," *Appl. Opt.*, vol. 26, pp. 2676–2682, July 1987.
[20] U. Bonse *et al.*, "Oscillatory structure of Laue case rocking curves," *Phys. Stat. Sol (a)*, vol. 43, pp. 487–492, 1977.
[21] D. Windisch and P. Becker, "Silicon lattice parameters as an absolute scale of length for high precision measurements of fundamental constants," *Phys. Stat. Sol (a)*, vol. 118, pp. 379–388, 1990.